Macromolecules

ARTICLE

pubs.acs.org/Macromolecules

Synthesis and Assembly of Butyl Rubber−Poly(ethylene oxide) Graft Copolymers: From Surface Patterning to Resistance to Protein Adsorption

Colin V. Bonduelle,[†] Solmaz Karamdoust,[†] and Elizabeth R. Gillies*[,†,‡]

[†]Department of Chemistry, The University of Western Ontario, 1151 Richmond Street, London, Canada, N6A 5B7

[‡]Department of Chemical and Biochemical Engineering, The University of Western Ontario, 1151 Richmond St., London, Canada, N6A 5B9

Supporting Information

ABSTRACT: The patterning of copolymers on surfaces is of interest both for a fundamental understanding of polymer assembly processes and for applications ranging from microelectronics to biomaterials. Graft copolymers can provide new opportunities to control polymer composition and architecture, thus opening possibilities for new assembly processes and patterns. In this work, the reaction of a butyl rubber derivative functionalized with activated carbonates along the polymer backbone was reacted with amine terminated poly(ethylene oxide) (PEO−NH_2) to provide butyl rubber−PEO graft copolymers. The high efficiency of this reaction allowed for control of the PEO content by the number of equivalents of PEO−NH_2 used and its molecular weight, providing a small library of graft copolymers. This approach also provided butyl rubber−PEO graft copolymers with unprecedentedly high PEO content. Thin films of the polymers, prepared by spin-casting were studied by a number of techniques including atomic force microscopy, polarized optical microscopy, profilometry, and confocal fluorescence microscopy following the adsorption of a fluorescent protein. Interestingly, as the PEO content of the copolymers increased, an evolution from complex micrometer scale to nanometer scale patterns was observed. This was accompanied by resistance of the surfaces to protein adsorption at high PEO content, demonstrating that function can evolve from the complex interplay of thermodynamic and kinetic factors governing the assembly of these thin films.

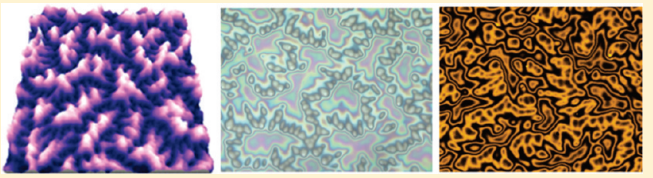

INTRODUCTION

Copolymers are of significant interest for a diverse range of applications, as they can impart the material with properties of both individual polymers as well as new properties of the combination.[1] This fruitful association is particularly relevant for block copolymers, which frequently self-assemble in the bulk, on surfaces, or in solution.[1−6] These assemblies have generated increasing interest over the past few decades for a diverse range of applications from drug delivery,[7,8] to catalysis,[9,10] and microelectronics.[11] For example, in surface science, block copolymers have been extensively used to achieve surface patterning by a bottom-up approach that exploits self-assembly during thin film formation.[12−17] Such patterns can be used in many applications including microelectronics,[18,19] biomaterials,[20−22] the generation of masks and templates,[23] and optical components.[24,25] Thus far, a significant body of research has been carried out on linear diblock and triblock copolymers, and the assembly behavior of these materials on surfaces is relatively well understood.[12,13,26−28] While comb-like or graft copolymer architectures have provided access to interesting spherical, hexagonal cylindrical, lamellar, flower and hyperbranched micellar morphologies after solution casting,[29−31] in general, there are relatively few examples involving these more complicated polymer architectures and their assemblies are less well understood.[12,32] However, they present interesting properties including the ability to finely tune their architectures by adjusting the grafting densities and relative chain lengths.[33−41]

In recent years, much research has emerged to suggest that polyisobutylene- (PIB-) based materials are highly promising for a number of biomedical applications.[42−44] For example, PIB−polystyrene (PS) triblock copolymers are currently being used as a drug eluting coating on TAXUS vascular stents.[44] Similar polymers are also being investigated as corneal shunts for the treatment of glaucoma,[45] as well as in synthetic aortic valves.[46] Furthermore, copolymers of PIB with hydrophilic polymers such as poly(*N*,*N*-dimethylacrylamide) or poly(ethylene oxide) (PEO) have been used to form membranes that can encapsulate cells while allowing the exchange of oxygen, nutrients, and secreted proteins such as insulin across the membrane.[47] However, optimization of the polymer chemistry and properties is still critical for many applications. For example, when PIB−PS was explored as a potential implant material in the urinary tract, significant attachment of uropathegenic species such as *Escherichia coli* 67 was observed, indicating that the

Received: May 2, 2011
Revised: July 18, 2011
Published: July 28, 2011

surface properties of the polymer were not ideal for this application.[48]

The incorporation of PEO into PIB-based materials is of particular interest as it is well-known to confer resistance of the surface to proteins,[49−51] which is a significant asset for biomedical devices and implants that often otherwise undergo rapid biofouling.[48,52,53] PIB−PEO linear block copolymers have previously been reported, but their syntheses are not straightforward as they typically involve a living cationic polymerization to form an end-functionalized PIB block,[54,55] followed by the coupling of PEO to the terminus using this functionality. For example, Guo and Kops coupled phenol-terminated PIB with tosylated PEO,[56] Roony reacted the same end-functionalized PIB with PEO by isocyanate chemistry,[57] and Kurian et al. used a coupling between silane functionalized PIB and allyl functionalized PEO.[58] However, each of these examples involved some degree of side reactions and/or low yields.

The grafting of PEO onto butyl rubber, a copolymer of isobutylene and small percentages of isoprene, has also been explored, but has been limited by challenges associated with solubility, low reactivity, and purification. For example, Kohjiya and co-workers have prepared butyl rubber−PEO graft copolymers with up to 24 wt % PEO by the reaction of chlorinated butyl rubber with the potassium salt of PEO monomethyl ether (m-PEO). However, they were not able to functionalize more than about 45% of the theoretical grafting sites.[59] Whitney, Parent and co-workers have explored the grafting of PEO onto bromobutyl using both the potassium salt of m-PEO as well as a carboxylate derivative.[60] Although recent catalytic approaches appear to be more promising,[61,62] incomplete couplings as well as side reactions such as eliminations to the conjugated diene were typically observed, resulting in a maximum of 30 wt % PEO. Our group has recently reported the preparation of butyl rubber−PEO graft copolymers by a mild and easy reaction sequence starting from the unhalogenated butyl rubber and using hydroxyl terminated m-PEO. This functionalization provided a PEO content of 8 wt %. Upon spin-casting, this polymer formed complex patterns that were revealed by fluorescence microscopy following the adsorption of fluorescent proteins.[63] This initial work has motivated the preparation of butyl rubber−PEO graft copolymers with a diverse range of PEO contents in order to better understand the patterning phenomenon and also to arrive at surfaces that resist the adsorption of proteins.

Described here is the extension of our butyl rubber functionalization chemistry to amine terminated PEO (PEO−NH_2). Use of PEO−NH_2 in place of m-PEO results in very high coupling efficiencies. This provides unprecedented control over the PEO grafting and the highest PEO contents reported thus far. Synthesis of a small library of butyl rubber−PEO graft copolymers with PEO content varying from 2 wt % to 65 wt % is reported, while to the best of our knowledge the highest previously reported content was 30 wt %. Thin films prepared by spin-casting these copolymers were studied, revealing an interesting evolution from micrometer to nanometer scale patterns with increasing PEO content. At higher PEO content, butyl rubber surfaces that resist the adsorption of proteins were obtained for the first time.

EXPERIMENTAL SECTION

General Procedures and Materials. Butyl rubber 402 (weight-average molecular weight (M_w) of 573 ± 62 KDa as measured by light scattering) composed of 2.2 mol % isoprene units was kindly provided by LANXESS and was converted to the activated derivative **1** by the previously reported method.[63] PEO−NH_2 of different molecular weights (750, 2000, and 5000 g/mol) were purchased from Iris Biotech GMBH (Marktredwitz, Germany). Silicon wafers were purchased from University Wafer (Boston, MA). Solvents were purchased from Caledon and all other chemicals were purchased from Sigma-Aldrich and were used without further purification unless otherwise noted. 4-(Dimethylamino)pyridine (DMAP) was purified by recrystallization in toluene before use. Dry toluene was obtained from a solvent purification system. ^{1}H NMR spectra were obtained in $CDCl_3$ at 400 MHz. NMR chemical shifts (δ) are reported in ppm and are calibrated against residual solvent signals of $CDCl_3$ (δ 7.26). Coupling constants (J) are reported in Hz. The percentage of functionalized isoprene units was determined from ^{1}H NMR, based on the relative integrations of the signals at 5.03 and 4.87 ppm corresponding to the alkene adjacent to the activated carbonate and the PEO carbamate product respectively (see Figure 1). The PEO content in wt % was determined from ^{1}H NMR, based on the relative integrations of the signals at 3.66 ppm and at 1.43 ppm corresponding to the PEO and isobutylene units respectively (see Figure 1). Differential scanning calorimetry (DSC) was performed on a Mettler Toledo DSC 822^e at a heating rate of 10 °C/min from −120 to +150 °C.

Molecular Weight Determination. The differential refractive index increment (dn/dc) values for each polymer in THF were determined using a Wyatt Optilab Rex refractive index detector and Wyatt Astra software. Next, time averaged light scattering intensities were measured for each polymer at a series of concentrations from 0.2 mg/mL to 1.2 mg/mL in THF using a Malvern Zetasizer Nano-S instrument. Toluene was used as a standard. Using this data, the M_w for each polymer was determined from the Rayleigh equation: $KC/R_\theta = (1/M_w + 2A_2C)P(\theta)$ using a Debye plot: KC/R_θ versus C, allowing $1/M_w$ to be determined as the y-intercept. C = polymer concentration; R_θ = excess Rayleigh ratio - the ratio of scattered and incident light intensity; A_2 = second viral coefficient which is a measure of solute−solvent interactions; $P(\theta)$ = scattering function which relates the angular variation in scattering intensity to the mean square radius of the particle; $K = 4\pi^2/\lambda_o{}^4 N_A[n_o(dn/dc)]^2$, where λ_0 = vacuum wavelength of incident light; N_A = Avogadro's number; n_0 = solvent refractive index.

Synthesis of Copolymer 2 and General Procedure for the Preparation of Copolymers 2−9. PEO−NH_2 with a molecular weight of 2000 g/mol (30 mg, 0.015 mmol) was dissolved in 10 mL of dry toluene at 60 °C. A solution of the butyl rubber derivative **1**[63] (750 mg, 0.28 mmol of 4-nitrophenylcarbonate units) in 15 mL of dry toluene was added dropwise to the reaction mixture. Next, a solution of 4-(dimethylamino)pyridine (50 mg, 0.40 mmol) in 10 mL of dry toluene was added and the resulting solution was stirred for 12 h at 60 °C. The solvent was evaporated *in vacuo* and the rubbery solid was washed one time with distilled water. The resulting material was precipitated twice from CH_2Cl_2 into acetone (1:10) to afford the copolymer **2**. (Yield = 85%.) ^{1}H NMR: δ 8.28 (d, 1.94H, J = 8.5), 7.40 (d, 1.94H, J = 8.5), 5.28 (s, 0.97H), 5.22 (s, 0.03H), 5.13 (s, 0.97H), 5.12 (s, 0.03H), 5.07 (s, 0.03H), 5.03 (s, 0.97H), 4.87 (s, 0.03H), 3.66 (s, 4H), 3.39 (s, 0.1H), 1.43 (s, 88H), 1.12 (s, 264H). PEO content (from ^{1}H NMR) = 2 wt %; T_g = −66 °C; T_m = 23 °C; M_w = 649 ± 19 KDa (dn/dc = 0.093 mL/g).

Synthesis of Copolymer 3. This copolymer was prepared by the same method as described above for copolymer **2** except that 0.1 equiv of PEO−NH_2 relative to the 4-nitrophenyl carbonates was used. (Yield = 77%.) ^{1}H NMR: δ 8.28 (d, 1.88H, J = 8.5), 7.40 (d, 1.88H, J = 8.5), 5.28 (s, 0.94H), 5.22 (s, 0.06H), 5.13 (s, 0.94H), 5.12 (s, 0.06H), 5.07 (s, 0.06H), 5.03 (s, 0.94H), 4.87 (s, 0.06H), 3.66 (s, 8H), 3.39 (s, 0.16H), 1.43 ppm (s, 88H), 1.12 (s, 264H). PEO content (from ^{1}H NMR) = 4 wt %; T_g = −67 °C; T_m = 24 °C; M_w = 676 ± 54 KDa (dn/dc = 0.084 mL/g).

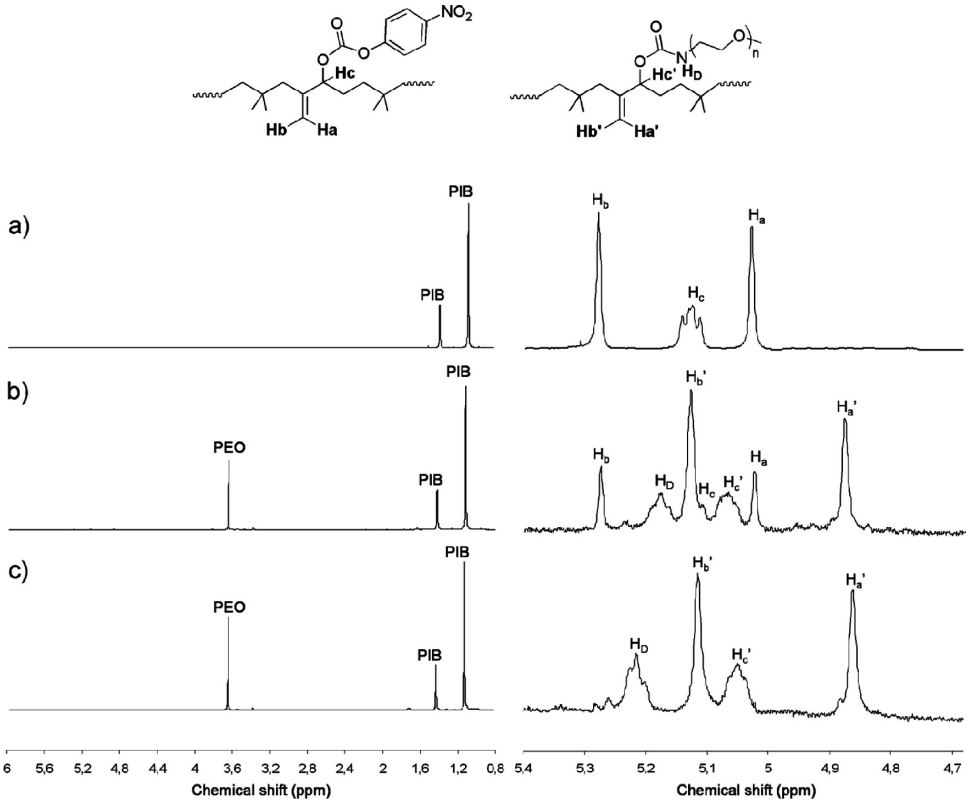

Figure 1. ^{1}H NMR spectra ($CDCl_3$, 400 MHz) of (a) activated butyl rubber **1**, (b) copolymer **6**, and (c) copolymer **7** showing how PEO content can be determined from the relative intensities of the PEO and PIB peaks and the reaction conversion can be assessed from the peaks in the region of 4.7−5.3 ppm.

Synthesis of Copolymer 4. This copolymer was prepared by the same method as described above for copolymer **2** except that 0.2 equiv of PEO−NH_2 relative to the 4-nitrophenyl carbonates was used. (Yield = 76%.) ^{1}H NMR: δ 8.28 (d, 1.7H, J = 8.5), 7.40 (d, 1.7H, J = 8.5), 5.28 (s, 0.86H), 5.22 (s, 0.14H), 5.13 (s, 0.86H), 5.12 (s, 0.14H), 5.07 (s, 0.14H), 5.03 (s, 0.86H), 4.87 (s, 0.14H), 3.66 (s, 13H), 3.39 (s, 0.25H), 1.43 (s, 88H), 1.12 (s, 264H). PEO content (from ^{1}H NMR) = 6 wt %; T_g = −62 °C; T_m = 28 °C; M_w = 657 ± 11 KDa (dn/dc = 0.070 mL/g).

Synthesis of Copolymer 5. This copolymer was prepared by the same method as described above for copolymer **2** except that 0.4 equiv of PEO−NH_2 relative to the 4-nitrophenyl carbonates was used. (Yield = 60%.) ^{1}H NMR: δ 8.28 (d, 1.32H, J = 8.5), 7.40 (d, 1.32H, J = 8.5), 5.28 (s, 0.68H), 5.22 (s, 0.32H), 5.13 (s, 0.68H), 5.12 (s, 0.32H), 5.07 (s, 0.32H), 5.03 (s, 0.68H), 4.87 (s, 0.32H), 3.66 (s, 30H), 3.39 (s, 0.6H), 1.43 (s, 88H), 1.12 (s, 264H). PEO content (from ^{1}H NMR): 12 wt %; T_g = −71 °C; T_m = 31 °C; M_w = 803 ± 38 KDa (dn/dc = 0.070 mL/g).

Synthesis of Copolymer 6. This copolymer was prepared by the same method as described above for copolymer **2** except that 0.8 equiv of PEO−NH_2 relative to the 4-nitrophenyl carbonates was used. (Yield = 51%) ^{1}H NMR: δ 8.28 (d, 0.5H, J = 8.5 Hz), 7.40 (d, 0.5H, J = 8.5), 5.28 (s, 0.25H), 5.22 (s, 0.75H), 5.13 (s, 0.25H), 5.12 (s, 0.75H), 5.07 (s, 0.75H), 5.03 (s, 0.25H), 4.87 (s, 0.75 H), 3.66 (s, 70H), 3.39 (s, 1.4H), 1.43 (s, 88H), 1.12 (s, 264H). PEO content (from ^{1}H NMR): 24 wt %; T_g = −69 °C; T_m = 30 °C; M_w = 872 ± 14 KDa (dn/dc = 0.065 mL/g).

Synthesis of Copolymer 7. This copolymer was prepared by the same method as described above for copolymer **2** except that 1.2 equiv of PEO−NH_2 relative to the 4-nitrophenyl carbonates was used and the resulting copolymer was purified by precipitation twice from THF into H_2O (1:2). (Yield = 49%.) ^{1}H NMR: δ 5.22 (s, 1H), 5.12 (s, 1H), 5.07 (s, 1H), 4.87 (s, 1H), 3.66 (s, 115H), 3.39 (s, 2.4H), 1.43 (s, 88H), 1.12 (s, 264H). PEO content (from ^{1}H NMR): 34 wt %; T_g = −62 °C; T_m = 39 °C; M_w = 971 ± 36 KDa (dn/dc = 0.050 mL/g).

Synthesis of Copolymer 8. This copolymer was prepared by the same method as described above for copolymer **2** except that 1.2 equiv of PEO−NH_2 of a molecular weight of 750 g/mol relative to the 4-nitrophenyl carbonates was used. (Yield = 75%.) ^{1}H NMR: δ 5.22 (s, 1H), 5.12 (s, 1H), 5.07 (s, 1H), 4.87 (s, 1H), 3.66 (s, 49H), 3.39 (s, 2.6H), 1.43 ppm (s, 88H), 1.12 (s, 264H). PEO content (from ^{1}H NMR): 18 wt %; T_g = −64 °C; T_m = 12 °C; M_w = 849 ± 34 KDa (dn/dc = 0.060 mL/g).

Synthesis of Copolymer 9. This copolymer was prepared by the same method as described above for copolymer **2** except that 1.2 equiv of PEO−NH_2 of a molecular weight of 5000 g/mol relative to the 4-nitrophenyl carbonates was used and the resulting copolymer was purified by precipitation twice from THF into H_2O (1:2). (Yield = 70%.) ^{1}H NMR: δ 5.22 (s, 1H), 5.12 (s, 1H), 5.07 (s, 1H), 4.87 (s, 1H), 3.66 (s, 425H), 3.39 (s, 2.4H), 1.43 (s, 88H), 1.12 (s, 264H). PEO content (from ^{1}H NMR): 65 wt %; T_g = −61 °C; T_m = 59 °C; M_w = 1550 ± 380 KDa (dn/dc = 0.055 mL/g).

Preparation of Thin Films. Silicon wafers were cut in small pieces (1 cm^2) and were cleaned by immersion in an H_2O_2/H_2SO_4 (1:2) solution overnight. They were then rinsed with deionized water and dried at 100 °C. Thin films of copolymers were prepared by spin-casting a solution of the material in CH_2Cl_2. Spin-casting conditions were 100 μL for 1 cm^2 of silicon wafer, 4000 rpm, 30 s.

Profilometry. The surfaces were imaged using a KLA Tencor P-10 Surface Profiler. Images were obtained by scanning 200 μm × 200 μm

Scheme 1. Synthesis of Butyl Rubber−PEO Graft Copolymers

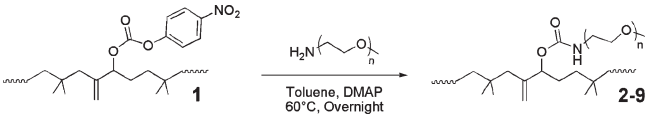

for each surface. The data were refined by using the software SPIP to get the 3D morphology.

Polarized Optical Microscopy. The surfaces were imaged with a Zeiss Axioplan compound microscope interfaced to a high-resolution color digital camera that allowed capture of digital images (magnification 20×). The images were taken in epi-illumination mode using a polarized optical microscope equipped with a linear polarizer. No analyzer nor waveplates were used.

Atomic Force Microscopy (AFM). The surfaces were visualized by an atomic force microscope (XE-100 microscope from psia). Images were obtained by scanning surfaces in a tapping mode using rectangular-shaped silicon cantilevers with a spring constant of 48 N/m. Data were then refined using the software Nanoscope. Roughness data correspond to the average Rq parameter calculated from four different whole surface areas of 20 μm × 20 μm. For the samples **7** - **9**, tapping mode to detect nanofeatures was performed with samples prepared from a 3 mg/mL polymer solution in CH_2Cl_2.

Protein Adsorption and Confocal Laser Scanning Microscopy. A 1 mg/mL solution of the rhodamine-fibrinogen conjugate[63] in 5 mM phosphate buffer, pH 7.2 was prepared. The surface was then immersed in this protein solution. After 30 min, nonadsorbed proteins were removed by washing the surface with buffer and water. The fluorescence was then evaluated by using an LSM 510 multichannel point scanning confocal microscope (Laser 543 nm and band-pass filter of 560−600 nm, magnification 20×). The settings on the instrument were kept constant for the comparison of all surfaces.

RESULTS AND DISCUSSION

Synthesis and Characterization of Butyl Rubber−PEO Graft Copolymers. Polymer **1** was prepared as previously reported from commercially available butyl rubber 402 by first epoxidation of the double bonds of the isoprene units using *m*-chloroperoxybenzoic acid, epoxide ring-opening followed by elimination to the exo double bond by treatment with HCl in toluene, then finally activation of the resulting hydroxyl groups with 4-nitrophenyl chloroformate.[63] These steps were mild, free of side reactions and essentially quantitative in their conversions. In previous work, we demonstrated that it was possible to prepare a butyl rubber−PEO graft copolymer by the reaction of hydroxyl terminated m-PEO with polymer **1**.[63] However, due to the limited nucleophilicity of the hydroxyl moiety, this reaction typically proceeded with only 15−20% conversion, providing copolymers with a PEO content of approximately 8 wt % in the case of an m-PEG of molecular weight (MW) 2000 g/mol. Attempts to increase this conversion by extending the reaction time or increasing the reaction temperature resulted in cross-linking or diene formation, side reactions that have been reported during the functionalization of halogenated butyl rubber.[59,64]

In contrast, changing to the more nucleophilic amine PEO−NH_2 (Scheme 1), while maintaining a reaction temperature of 60 °C and a reaction time of 12 h, resulted in a dramatic improvement in the reaction conversion, resulting in the functionalization of essentially 100% of the isoprene units, as determined within the detection limits of ^{1}H NMR spectroscopy. To the best of our knowledge, this is the first reported method that enables the introduction of PEO to each isoprene unit along the butyl rubber backbone. The ability to control the final PEO content in the graft copolymers via the number of equivalents of PEO−NH_2 was also investigated, as such control as not been demonstrated in the previous syntheses of butyl rubber−PEO graft copolymers.[59,60,65,66] In addition, diverse PEO contents were obtained by using PEO−NH_2 with varying MWs of 750, 2000, or 5000 g/mol. As shown in Table 1, a small library of eight copolymers was prepared.

Purification of each graft copolymer from ungrafted PEO−NH_2 was accomplished by first washing with water then by precipitations. Precipitation was achieved by using a solvent that was a nonsolvent for butyl but a good solvent for PEO. Acetone was used in the case of low PEO content, while H_2O was required in the case of higher PEO content as it is a stronger nonsolvent for the butyl. The yields ranged from 49% to 85% and were logically lower for the copolymers with higher PEO content because of their partial solubilities in water. Indeed, one can assume that if this purification isolated only a selective fraction from the precipitation, it would be the fraction with lower PEO content, as more PEO would make the copolymer more soluble in water. Therefore, our purification allowed isolation of the copolymers with the lower limits on the PEO content.

After removal of ungrafted PEO from the graft copolymer products, they were characterized by ^{1}H NMR spectroscopy, DSC, SEC, and light scattering. Following conjugation of the PEO−NH_2 and thus conversion of the activated carbonates to carbamates, the ^{1}H NMR peaks corresponding to the exo alkene and the C−H in the α-position to the activated carbonate in the region from 4.5 to 5.5 ppm were observed to shift significantly as shown in Figure 1. This allowed for quantification of the percentage of functionalized isoprene units (Figure 1, Table 1). In addition, as previously reported,[59] we compared the ^{1}H NMR integrations of the peaks corresponding to the PEO at 3.66 ppm and the polyisobutylene units at 1.43 ppm to estimate the PEO content (Figure 1).

In order to obtain relatively low PEO content materials, copolymers **2**, **3**, and **4** were prepared using 0.05, 0.1, and 0.2 equiv of PEO−NH_2 relative to the activated carbonates in polymer **1**. On the basis of ^{1}H NMR analyses, these reactions resulted in the functionalization of approximately 3%, 6%, and 14% of the isoprene units, providing polymers with 2, 4, and 6 wt % PEO respectively (Table 1). Copolymers **5** and **6** were prepared using 0.4 and 0.8 equiv of PEO−NH_2. This resulted in the functionalization of approximately 32% and 75% of the isoprene units, providing copolymers with 12 and 24 wt % PEO. In addition, with the aim of achieving unprecedentedly high weight fractions of PEO in the products, polymer **1** was reacted with 1.2 equiv of PEO−NH_2 having a molecular weight of 750, 2000, or 5000 g/mol. Subsequently, ^{1}H NMR analyses revealed that essentially 100% of the isoprene units were functionalized in each case, resulting in PEO contents of 18, 34, and 65 wt % for copolymers **8**, **7**, and **9** respectively. Overall, as the grafting reactions proceeded with high yields based on ^{1}H NMR analysis of the isolated products, isolation of a nonrepresentative fraction of the reaction products in the precipitation process did not seem to be an issue. Until now, the highest PEO contents were previously reported by Yamashita et al. using PEO of 750 g/mol and 2000 g/mol to prepare graft copolymers with 10 and 24 wt % respectively[59] and by Guillen-Castellanos et al. with PEO of 5000 g/mol providing 30 wt % PEO[65] (Table 2). It should be

Table 1. Characterization of Library or Butyl Rubber−PEO Graft Copolymers

copolymer	PEO−NH_2 MW (g/mol)	PEO−NH_2 equiv	% functionalized isoprene units[a]	PEO content[b] (wt %)	M_w (KDa)[c]	T_m (°C)[d]
2	2000	0.05	3	2	650 ± 19	23
3	2000	0.1	6	4	676 ± 54	24
4	2000	0.2	14	6	660 ± 11	28
5	2000	0.4	32	12	800 ± 38	31
6	2000	0.8	75	24	870 ± 14	30
7	2000	1.2	100	34	970 ± 36	39
8	750	1.2	100	18	850 ± 34	12
9	5000	1.2	100	65	1550 ± 380	59

[a] From ^{1}H NMR, based on the relative integrations of the signals at 5.03 and 4.87 ppm corresponding to the alkene adjacent to the activated carbonate and the PEO carbamate product respectively (see Figure 1). [b] From ^{1}H NMR, based on the relative integrations of the signals at 3.66 ppm and at 1.43 ppm corresponding to the PEO and isobutylene units, respectively. [c] From light scattering. [d] From DSC analysis.

Table 2. Comparison of the Current PEO Grafting Results with Those Previously Reported

	PEO content (wt %) of graft copolymers	
MW (g/mol) of conjugated PEO	previous work (best result)	current study
750	10[59,a]	18
2000	24[59,a]	34
5000	30[65,b]	65

[a] From chlorobutyl containing 2.0 mol % of halogen. [b] From bromobutyl containing 1.1 mol % isoprene.

noted that in the latter case, this graft copolymer was prepared from a butyl polymer containing only 1.1 mol % of halogenated monomers in comparison with the 2.2 mol % of activated monomers used in the current work. Nevertheless, the PEO content was lower than the theoretically achievable value of 49 wt %. Although our reaction sequence involves multiple steps, the high PEO contents and level of control over this content can be attributed to the highly efficient grafting reaction.

The thermal properties of copolymers **2**−**9** were measured by DSC analyses. PEO homopolymer of 2000 g/mol is crystalline with a T_m of 58 °C, whereas butyl rubber is noncrystalline with a T_g of −73 °C (Supporting Information). Despite the widely varying PEO content of copolymers **2**−**9**, no significant changes or trends in the T_gs were observed. In contrast, as expected based on previous reports,[65] the T_m of the PEO was significantly reduced by incorporation into the graft copolymers (Table 1). At low PEO content, the T_m was much lower than the T_m of pure PEO of the same molecular weight. For example, copolymer **2** containing only 2 wt % PEO had a T_m of only 23 °C. However, the T_m increased with increasing PEO content up to 39 °C for copolymer **7**, containing 34 wt % PEO. The highest T_m of 59 °C was measured for copolymer **9**, which had 100% of the isoprene units functionalized with PEO of 5000 g/mol. This T_m was very similar to the T_m of 61 °C for the corresponding PEO homopolymer. The lowest T_m of 12 °C was measured for polymer **8**, which contained 100% of the isoprene units functionalized with PEO of 750 g/mol. This low T_m is not surprising in light of the T_m of 22 °C for the corresponding PEO homopolymer. Overall, these results suggest that the presence of higher PEO content and higher PEO MW results in higher T_m, likely due to the ability of these copolymers to form larger PEO domains which possess crystallinities more similar to those of pure PEO. These DSC results were also useful in confirming the absence of ungrafted PEO in the graft copolymers. The presence of free PEO in unpurified samples of the graft copolymers leads to an additional melting peak at the temperature expected for the corresponding PEO homopolymer (Supporting Information). This extra melting peak was not observed in the DSC traces of any of the purified polymers **2**−**9**.

SEC analysis of butyl rubber−PEO graft copolymers containing significant PEO content was problematic, an issue that has previously been reported.[59] Therefore, the M_ws of the graft copolymers were determined by light scattering analyses in the absence of a column. First, the differential refractive index increment (dn/dc) was measured for each polymer in THF using a refractive index detector, and then the time averaged light scattering intensities for each polymer were measured as a function of concentration and their molecular weights were determined using Debye plots (Supporting Information). As shown in Table 1, the M_ws measured by this method increased as expected with increasing PEO content. For example, copolymer **2** containing 2 wt % PEO was found to have a M_w of 649 KDa, a value close to the 573 KDa measured for the butyl rubber 402 starting material, while copolymer **7** containing 34 wt % PEO had a M_w of 971 KDa. Because of the nature of the light scattering technique, these data should reflect the true M_ws of the samples in contrast to those determined by relative calibrations, which more closely reflect the hydrodynamic size and can be influenced by other effects such as interactions with the column. The main drawback is that in the absence of separation by the column, it was not possible to obtain information on the polydispersity indices of the samples.

Preparation and Study of Thin Films of Copolymer 2−7. In recent work, we found that a butyl rubber−PEO graft copolymer containing 8 wt % PEO, prepared by the reaction of hydroxyl terminated PEO with polymer **1**, formed novel micrometer scale patterns when spin-cast on surfaces.[63] These patterns were revealed by AFM, polarized optical microscopy and fluorescence confocal microscopy following the adsorption of fluorescent proteins. The pattern formation was attributed to both kinetic factors such as the freezing of Marangoni instabilities[67] as well as thermodynamic factors such as phase separation.[14] However, the exact driving forces for pattern formation and the nature of the protein adsorption were not fully elucidated. Therefore, it was of significant interest to study the evolution of the patterns with varying PEO content and MW.

First, thin films of copolymer **2** containing 2 wt % PEO were prepared by spin-casting CH_2Cl_2 solutions with concentrations

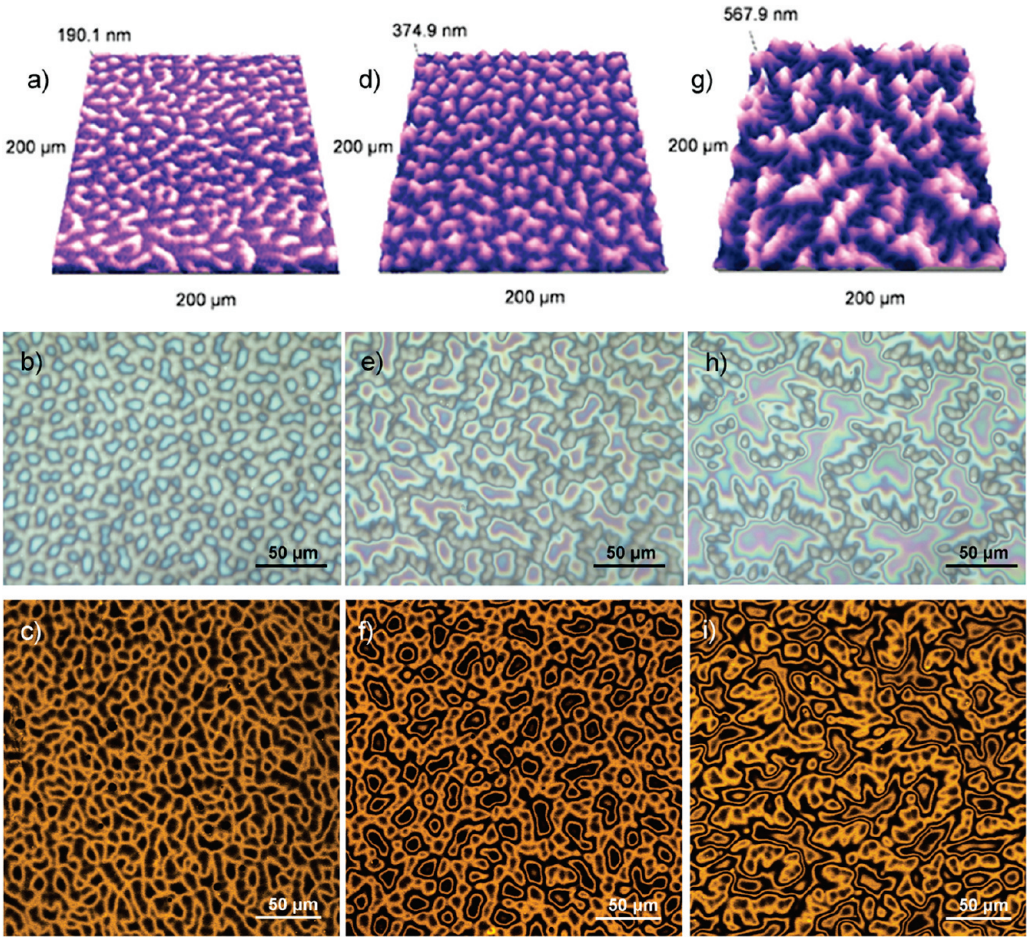

Figure 2. Analyses of thin films obtained after spin-casting a solution of graft copolymer **2** (in CH_2Cl_2) on silicon wafers: (a−c) 10 mg/mL; (d−f) 15 mg/mL; (g−i) 20 mg/mL. Top line: profilometry analyses revealing topographical features increase with concentration. Second line: patterns revealed by polarized optical microscopy are consistent with those obtained by profilometry. Third line: fluorescence confocal microscopy images (543 nm) following adsorption of a rhodamine−fibrinogen conjugate correlate with above images.

of 10 mg/mL, 15 or 20 mg/mL on clean silicon wafers. As observed in the previous study, AFM revealed full surface coverage of the silicon wafer, as well as topographical features, but these features were larger than the scale of typical AFM images, making pattern visualization challenging. However, as shown in Figure 2, profilometry successfully revealed distinct micrometer scale surface features with heights on the order of 20−200 nm and the patterns evolved with concentration. Larger features were observed at higher concentrations. The patterns could also be visualized by polarized optical microscopy (Figure 2b,e,h) and there was agreement between the nature of the profilometry and optical microscopy images. Given the profilometry and AFM results demonstrating surface topography, the colors in the images are almost certainly generated by variations in the film thicknesses of the thin films on the flat silicon wafer. This is due to optical interferences that are thickness dependent.

As PEO is well-known to resist the adsorption of proteins,[49−51] it was initially hypothesized that by studying the adsorption of fluorescent proteins, some insight might be gained into the role of polymer phase separation in the pattern formation. Thus, the surfaces were imaged by fluorescence confocal microscopy following immersion in a solution of rhodamine-labeled fibrinogen,[63] a protein commonly evaluated in protein adsorption studies.[68] As shown in Figure 2, complex patterns similar to those observed with our previously reported graft copolymer[63] were observed. Comparison of these patterns with the profilometry images

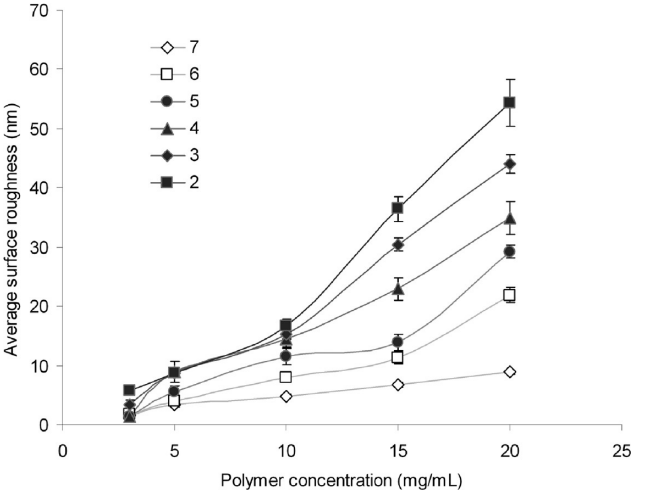

Figure 3. Average surface roughness values for thin films prepared from polymers **2**−**7** as a function of concentration, obtained from an AFM analyses.

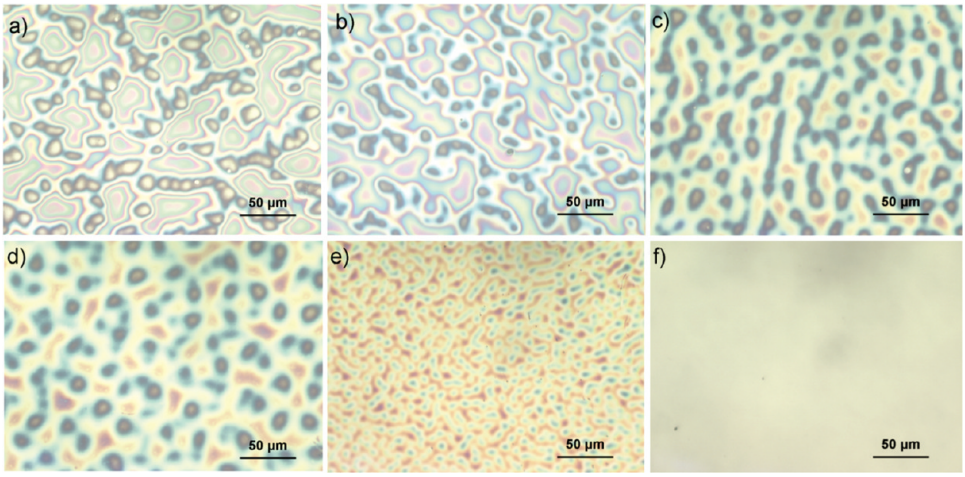

Figure 4. Polarized optical microscopy images of thin films of graft copolymers spin-cast from CH_2Cl_2 (20 mg/mL): (a) copolymer **2**; (b) copolymer **3**; (c) copolymer **4**; (d) copolymer **5**; (e) copolymer **6**; (f) copolymer **7**.

indicates that aspects of the topography are revealed in the protein adsorption, but this correlation is not as simple as proteins adsorbing specifically to peaks or valleys on the surface. Although, the thermal data suggested phase separation of the polymers in the bulk, the casting of films from solution, and the rapid evaporation of the solvent in this process can have a significant effect. The nanoscale dimensions of the individual polymer chains and their relatively low PEO content, make it unlikely that in the case of copolymer **2** the large micrometer scale regions lacking fluorescence correspond entirely to PEO. This suggests that some combination of topography and phase separation resulting in the possible formation of butyl-enriched and PEO-enriched domains may play a role in the protein adsorption. For example, fibrinogen has been shown previously to adsorb preferentially at the interface between two materials.[69,70]

To gain more insight into the nature and origin of the pattern formation, the influence of the PEO content on the resulting thin films was studied. First, AFM was used to determine the average surface roughness as a function of both the PEO content and the copolymer concentration. Thin films of copolymers **2**−**7** were prepared from CH_2Cl_2 solutions at concentrations ranging from 3 to 20 mg/mL. As shown in Figure 3, the surface roughness was indeed strongly influenced by both the PEO content and the copolymer concentration. The surface roughness decreased significantly with increasing PEO content, from greater than 50 nm for copolymer **2** spin-cast at 20 mg/mL to less than 10 nm measured for copolymer **7** at the same concentration. The roughness also increased with concentration, most notably for the polymers with lowest PEO content.

Polarized optical microscopy was also used to probe the evolution of the patterns with varying PEO content. Images of thin films prepared from copolymers **2**−**7** at a concentration of 20 mg/mL in CH_2Cl_2 are shown in Figure 4. As suggested by the surface roughness measurements, an evolution in the patterns with increasing PEO content was observed. Although polarized optical microscopy cannot directly reveal topographical information, the images suggested that larger features were obtained at lower PEO contents, such as for copolymers **2** and **3**. The sizes of these features consistently decreased for copolymers **4**, **5**, and **6**, and eventually disappeared for copolymer **7**. The same trends were observed for films prepared from copolymer solutions at 10 and 15 mg/mL (Supporting Information). In light of these results, it was of interest to evaluate the pattern formation resulting from pure butyl rubber and pure PEO spin-cast from CH_2Cl_2. PEO spin-cast from CH_2Cl_2 consistently provides smooth films (surface roughness <2 nm), without patterns. In contrast, pure butyl rubber has limited solubility in CH_2Cl_2 and does not provide thin films but rather islands of aggregated polymer on the surface (Supporting Information). However, smooth films of butyl rubber can be prepared by spin-casting from hexane, verifying that this effect is not dominated by the substrate. In addition, previous work has shown that noncovalent blends of butyl rubber and PEO at similar weight ratios to polymers **3** and **4** do not produce regular surface patterns.[63] Therefore, the covalent graft copolymer containing both butyl rubber and PEO is essential for pattern formation.

The adsorption of the fluorescent rhodamine-fibrinogen conjugate to the films spin-cast from copolymers **2**−**7** was also evaluated. The patterns obtained from copolymer solutions spin-cast at 20 mg/mL are shown in Figure 5. Overall, these patterns were in agreement with the polarized optical microscopy images but they revealed increased complexity, suggesting that additional factors such as partial phase separation might result in the adsorption of proteins to selected regions of the surface. Particularly complex and novel patterns were observed at low PEO content, such as the apparent "worm-like" structures containing spherical species that were observed for copolymer **4** (Figure 5c). It is also noteworthy that in agreement with the lack of pattern formation observed by AFM or polarized optical microscopy, thin films of copolymers **6** and **7** did not adsorb significant levels of fluorescent protein and thus fluorescent patterns were not observed. Despite the lack of topographical patterns formed by these polymers, the resistance to protein adsorption is still rather remarkable as copolymers **6** and **7** contain only 24 and 34 wt % of PEO respectively. With the knowledge that proteins adsorb extensively to surfaces prepared from pure butyl[48,71] and not to PEO surfaces,[49−51] these results suggest that the surfaces prepared from these copolymers are capable of presenting sufficient amounts of PEO at the surface to repel proteins. Similar trends in the protein patterning were also observed for thin films cast from copolymers **2**−**7** at concentrations of 10 and 15 mg/mL (Supporting Information).

Comparison of Thin Films Prepared from Copolymers 7−**9.** While the above study evaluated the effect of PEO content

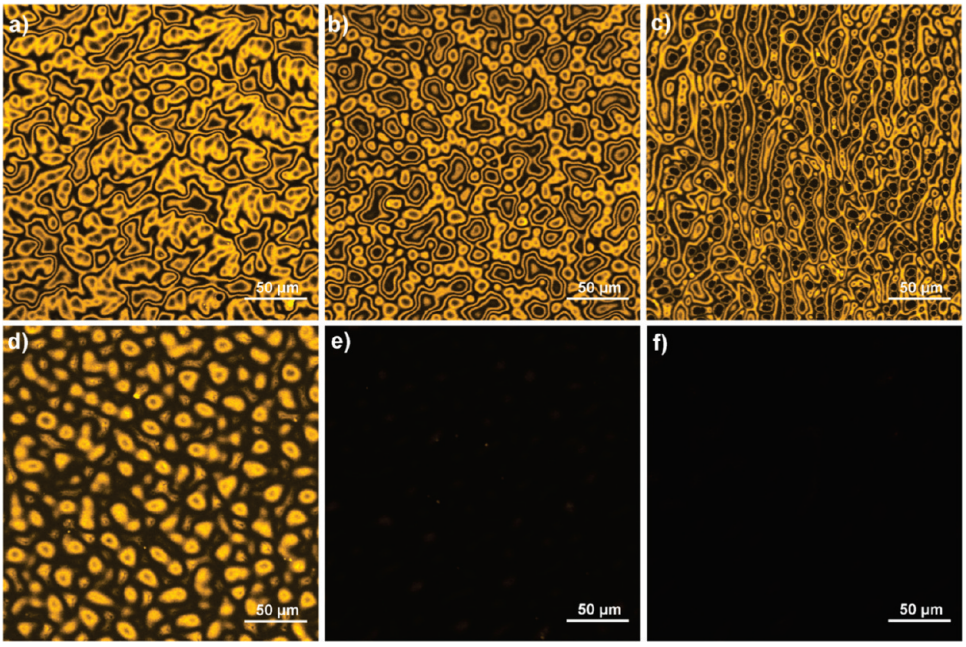

Figure 5. Fluorescence confocal microscopy images (543 nm) of thin films (spin-cast at 20 mg/mL from CH_2Cl_2) following adsorption of a rhodamine-fibrinogen conjuguate. Key: (a) copolymer **2**; (b) copolymer **3**; (c) copolymer **4**; (d) copolymer **5**; (e) copolymer **6**; (f) copolymer **7**.

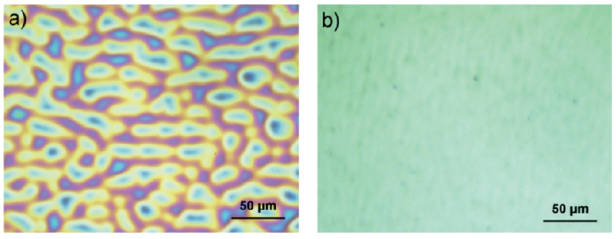

Figure 6. Polarized optical microscopy images of thin films of graft copolymers (a) **8** and (b) **9**, spin-cast from CH_2Cl_2 (20 mg/mL).

while keeping the PEO MW constant at 2000 g/mol, it was also of interest to evaluate the effects of PEO MW by comparing thin films prepared from copolymers **8** and **9** with those from copolymer **7**. First, films were prepared by spin-casting CH_2Cl_2 solutions with concentrations of 10, 15, or 20 mg/mL on clean silicon wafers. Polarized optical microscopy revealed that more significant features were obtained for copolymer **8** that was fully functionalized with a PEO of MW 750 g/mol (Figure 6a) in comparison with copolymer **7** (Figure 4f) containing PEO of MW 2000 g/mol. Copolymer **9** (Figure 6b), fully functionalized with PEO of MW 5000 g/mol exhibited much less texture than copolymer **8**, but interestingly more texture than copolymer **7**. In accordance with the DSC results, this texture may be due to the crystallinity of the PEO domains. As for copolymer **7**, no significant protein adsorption was observed for polymers **8** and **9** (Supporting Information). This is particularly noteworthy in the case of polymer **8**, which contains only 18 wt % PEO and did exhibit patterns in the polarized optical microscopy images.

Despite the lack of evidence for micrometer scale patterning for copolymers **7** and **9**, butyl rubber and PEO are nevertheless incompatible, and previous studies involving small-angle X-ray scattering (SAXS) and dynamic mechanical analyses have suggested that these polymers undergo phase separation at the

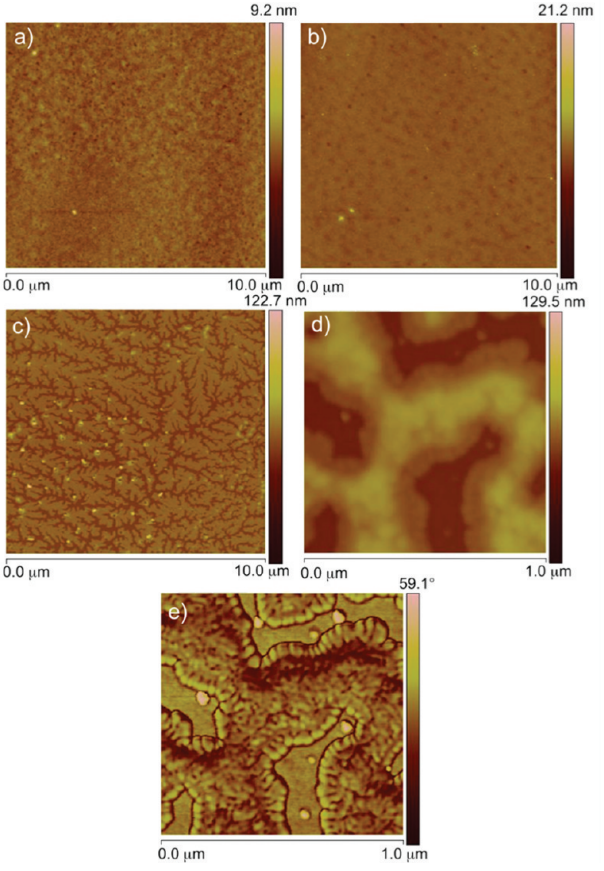

Figure 7. AFM analysis (tapping mode) of the thin films spin-cast on silicon wafers: (a) topography of copolymer **7**; (b) topography of copolymer **8**; (c) topography of copolymer **9**; (d) topography of copolymer **9** zooming in on the dendritic nanostructures; (e) phase imaging of copolymer **9** zooming in on the dendritic nanostructures.

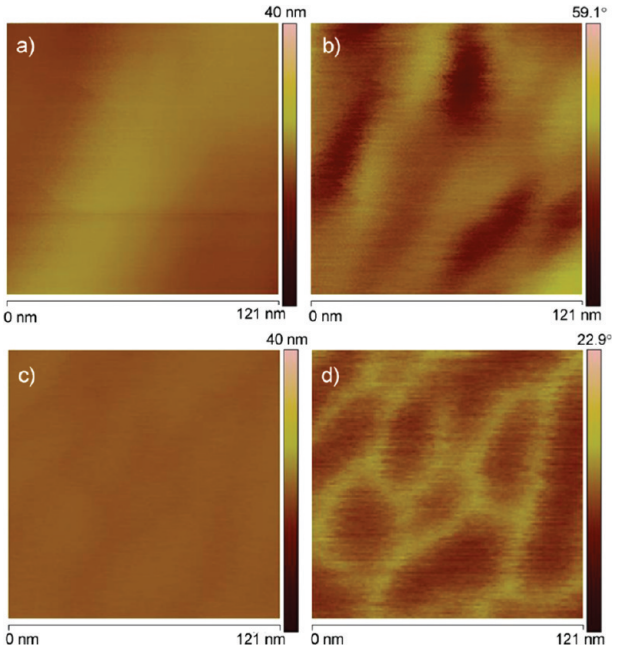

Figure 8. AFM analyses of the thin film obtained after spin-casting a solution of **9**. Before annealing: (a) topography; (b) phase contrast. After annealing: (c) topography; (d) phase contrast.

nanometer scale.[66] Therefore, to obtain nanometer scale information, these surfaces were further investigated by AFM. As shown in Figure 7a, AFM analysis of the thin film prepared from copolymer **7**, with grafts of PEO of 2000 g/mol, revealed a relatively flat surface that presented no significant patterns or irregularities. AFM of films from copolymer **8** (Figure 7b), with grafts of PEO of 750 g/mol, revealed a more inhomogeneous surface, certainly an intermediate step toward the patterns previously evidenced at lower PEO contents for polymers **2**−**5**, and in agreement with the polarized optical microscopy images. Finally, AFM analyses of the thin film prepared from copolymer **9**, with grafts of PEO of 5000 g/mol and a high PEO content of 65%, showed "dendritic-like" nanostructures (Figure 7c). Interestingly, while the roughness measured for the thin films made with copolymers **7** or **8** was low (below 2 nm for both), thin films from copolymer **9** exhibited a higher roughness of 4.9 nm.

Additional AFM imaging was performed on films of copolymer **9** to further probe the fine dendritic structures. As shown in parts d and e of Figure 7, while the topographical image provided limited information, it was possible to obtain a phase image of the dendritic nanostructures. This phase image revealed nanodomains of approximately 50 nm in diameter, which were assembled in a complex manner to form the dendritic structures, possibly again a result of the PEO crystallinity. As shown in Figure 8, further investigation at the nanometer scale suggested polymer phase separation within the ellipsoidal structures that may correspond to the butyl rubber and PEO domains of individual polymer chains. Annealing these surfaces at 100 °C overnight, while reducing surface roughness, accentuated this phase separation, consistent with a thermodynamically driven assembly process. It should be noted that no clear phase separation could be observed in the films of copolymers **2**−**7** by AFM.

Using the information on pattern formation from the studies above, insights into the factors leading to these micrometer and nanometer scale patterns have been gained. The solvent-assisted deposition of the materials on surfaces is a complex process with three different types of interactions involved: molecule−molecule, molecule-solvent and molecule−substrate.[14] These interactions are often weak and the morphologies of the resulting films are not always easy to predict. It is known that after drop deposition, the different interfaces of the system create a destabilized layer with a high surface roughness.[72] This roughness tends to decrease during solvent evaporation until the thin layer is formed. Solvent plays a crucial role during this step involving the leveling of the surface roughness,[67] and in the case of solvent-rich films, rapid evaporation can freeze states of the destabilized layers created by Marangoni instabilities.[73] The significant surface roughness increases with increasing concentrations of copolymers **2**−**7** (Figure 3) are in agreement with a kinetic freezing of a destabilized solvent-rich layer,[67] particularly for copolymers with low PEO content. Furthermore, it had been shown that the patterning of these graft copolymers is highly dependent on the solvent, with films spin-cast from hexane not revealing patterns.[63] As a high vapor pressure of the solvent is critical for the freezing of kinetic instabilities, and that of hexane is much lower than that of CH_2Cl_2, this also supports this kinetic mechanism. Furthermore, the kinetic trapping mechanism is known to generally produce micrometer scale patterns, which is clearly the dimension observed for polymers **2**−**5**.[14]

On the other hand, the disappearance of the concentration effect and of micrometer scale patterns suggest that kinetic trapping is not the dominant mechanism of pattern formation for polymers **6**−**9**, which possess higher PEO contents. For these polymers, phase separation seems to dominate, leading to the gradual disappearance of micrometer scale patterning and the emergence of nanometer scale patterning as evidenced by AFM for polymer **9**. Indeed, macromolecular assembly during thin film formation involving amphiphilic copolymers generally leads to smaller scale patterning than that created by the kinetic effect.[14,15] Thus, it appears that through the series of butyl rubber−PEO graft copolymers evaluated in this study an evolution from a primarily kinetically governed patterning to one governed by phase separation was observed. This evolution can possibly be attributed to an increased solubility of the polymers in CH_2Cl_2 with increasing PEO content, which may decrease the instabilities that can be trapped during spin coating. At the same time, an increase in the PEO content may increase the role of polymer phase separation. This evolution from micrometer to nanometer scale patterns was also accompanied by a change from complex patterns of protein adsorption, a result likely attributable to topographical effects and partial phase separation, to resistance to protein adsorption at higher PEO content.

■ CONCLUSIONS

In conclusion, a new synthetic approach was developed for the grafting of PEO onto the butyl rubber backbone to form butyl rubber−PEO graft copolymers. This method was used to generate a small library of eight copolymers with varying PEO content by tuning both the number of equivalents of PEO−NH_2 grafted as well as the lengths of the PEO chains. These copolymers had PEO content ranging up to 65 wt %, nearly 2-fold higher than the butyl rubber−PEO graft copolymers previously reported. This result was possible due to the high efficiency of the grafting reaction. Thin films of the copolymers were studied by AFM, profilometry, polarized optical microscopy and fluorescence confocal microscopy following the adsorption of fluorescent proteins. As the PEO content was increased, an evolution

from micrometer scale patterning that was primarily kinetically governed, to nanometer scale patterning likely governed by thermodynamic phase separation was observed. In addition, at high PEO content, resistance to protein adsorption was observed, a property that may be a significant asset for the application of these materials in biomedical devices. Further study of this effect and potential applications are currently underway.

■ ASSOCIATED CONTENT

Supporting Information. ^{1}H NMR spectra of copolymers **2**−**9**, representative DSC traces of an unpurified and purified graft copolymer, additional polarized optical microscopy and fluorescence confocal microscopy images, and details of the molecular weight analysis, including light scattering Debye plots. This material is available free of charge via the Internet at http://pubs.acs.org/.

■ ACKNOWLEDGMENT

We thank LANXESS Inc. for funding of this work and for providing samples of butyl rubber. The Ontario Centres of Excellence and the Natural Sciences and Engineering Research Council of Canada are also thanked for funding. Surface Science Western (Heng-Yong Nie and Wei Zhou) is thanked for assistance with AFM imaging and the Biotron Imaging Facility is thanked for help with optical imaging. We thank Darryl K. Knight for help with DSC analyses.

■ REFERENCES

(1) Lazzari, M.; Liu, G.; Lecommandoux, S. *Block Copolymers in Nanoscience*; Wiley-VCH: Weinheim, Germany, 2006.
(2) Hayward, R. C.; Pochan, D. J. *Macromolecules* **2010**, *43*, 3577–3584.
(3) Giacomelli, C.; Schmidt, V.; Aissou, K.; Borsali, R. *Langmuir* **2010**, *26*, 15734–15744.
(4) Grzelczak, M.; Vermant, J.; Furst, E. M.; Liz-Marzan, M. L. *ACS Nano* **2010**, *4*, 3591–3605.
(5) Lin, Y.; Boker, A.; He, J.; Sill, K.; Xiang, H.; Abetz, C.; Li, X.; Wang, J.; Emrick, T.; Long, S.; Wang, Q.; Balazs, A.; Russel, T. P. *Nature* **2005**, *434*, 55–59.
(6) Whitesides, G. M.; Grzybowski, B. *Science* **2002**, *295*, 2418–2421.
(7) Soussan, E.; Cassel, S.; Blanzat, M.; Rico-Lattes, I. *Angew. Chem., Int. Ed.* **2008**, *48*, 274–288.
(8) Pan, D.; Turner, J. L.; Wooley, K. L. *Chem. Commun.* **2003**, 2400–2401.
(9) Nuyken, O.; Weberskirch, R.; Kotre, T.; Schoenfelder, D.; Woerndle, A. In *Polymeric Materials in Organic Synthesis and Catalysis*; Buchmeiser, M. R., Ed.; Wiley-VCH: Weinheim, Germany, 2003; p 277−304.
(10) Okhapkin, I. M.; Makhaeva, E. E.; Elena, E.; Khokhlov, A. R. *Adv. Polym. Sci.* **2006**, *195*, 177–210.
(11) Ruokolainen, J.; Makinen, R.; Torkkeli, M.; Makela, T.; Serimaa, R.; Brinke, G. T.; Ikkala, O. *Science* **1998**, *280*, 557–560.
(12) Hamley, I. W. *Prog. Polym. Sci.* **2009**, *34*, 1161–1210.
(13) Darling, S. B. *Prog. Polym. Sci.* **2007**, *32*, 1152–1204.
(14) Palermo, V.; Samori, P. *Angew. Chem., Int. Ed.* **2007**, *46*, 4428–4432.
(15) Segalman, R. A. *Mater. Sci. Eng. Res.* **2005**, *48*, 191–226.
(16) Shimomura, M.; Sawadaishi, T. *Curr. Opin. Colloid Interface Sci.* **2001**, *6*, 11–16.
(17) Nie, Z.; Kumacheva, E. *Nature Mater.* **2008**, *7*, 277–290.
(18) Singh, T. B.; Sariciftci, N. S. *Annu. Rev. Mater. Res.* **2006**, *36*, 199–230.
(19) Ho-Cheol, K.; Hinsberg, W. D. *J. Vac. Sci. Technol., A* **2008**, *26*, 1369–1382.
(20) Roach, P.; Eglin, D.; Rohde, K.; Perry, C. C. *J. Mater. Sci.: Mater. Med.* **2007**, *18*, 1263–1277.
(21) Hollister, S. J. *Nat. Mater.* **2005**, *4*, 518–524.
(22) Théry, M.; Racine, V.; Piel, M.; Pépin, A.; Dimitrov, A.; Chen, Y.; Sibarita, J.-P.; Bornens, M. *Proc. Natl. Acad. Sci. U.S.A.* **2006**, *103*, 19771–19776.
(23) Park, M.; Harrison, C.; Chaikin, P. M.; Register, R. A.; Adamson, D. H. *Science* **1997**, *276*, 1401–1404.
(24) Campbell, M.; Sharp, D. N.; Harrison, M. T.; Denning, R. G.; Tuberfield, A. J. *Nature* **2000**, *404*, 53–56.
(25) Valkama, S.; Kosonen, H.; Ruokolainen, J.; Haatainen, T.; Torkkeli, M.; Serimaa, R.; ten Brinke, G.; Ikkala, O. *Nat. Mater.* **2004**, *3*, 872–876.
(26) Dalnoki-Veress, K.; Forrest, J. A.; Stevens, J. R.; Dutcher, J. R. *Physica A* **1997**, *239*, 87–94.
(27) Walheim, S.; Böltau, M.; Mlynek, J.; Krausch, G.; Steiner, U. *Macromolecules* **1997**, *30*, 4995–5003.
(28) Sprenger, M.; Walheim, S.; Budkowski, A.; Steiner, U. *Int. Sci.* **2003**, *11*, 225–235.
(29) Kishida, A.; Seto, F.; Hiwatari, K.; Serizawa, T.; Muraoka, Y.; Akashi, M. *Chem. Lett.* **1999**, 1221–1222.
(30) Ruokolainen, J.; Saariaho, M.; Ikkala, O. *Macromolecules* **1999**, *32*, 1152–1158.
(31) Lanson, D.; Schappacher, M.; Borsali, R.; Deffieux, A. *Macromolecules* **2007**, *40*, 9503–9509.
(32) van Zoelen, W.; Ten Brinke, G. *Soft Matter* **2009**, *5*, 1568–1582.
(33) Zhang, X.; Shen, Z.; Feng, C.; Yang, D.; Li, Y.; Hu, J.; Lu, G.; Huang, X. *Macromolecules* **2009**, *40*, 4249–4256.
(34) Gu, L.; Shen, Z.; Feng, C.; Y., L.; Lu, G.; Huang, X. *J. Polym. Sci., Part A: Polym. Chem.* **2008**, *46*, 4056–4069.
(35) Wan, S.; Jiang, M.; Zhang, G. *Macromolecules* **2007**, *40*, 5552–5558.
(36) Balomenou, I.; Bokias, G. *Langmuir* **2005**, *21*, 9038–9043.
(37) Pitsikalis, M.; Woosward, J.; Mays, J. W. *Macromolecules* **1997**, *30*, 5384–5389.
(38) Pispas, S.; Hadjichristidis, N.; Mays, J. W. *Macromolecules* **1996**, *29*, 7378–7385.
(39) Bougard, F.; Giacomelli, C.; Mespouille, L.; Borsali, R.; Dubois, P.; Lazzaroni, R. *Langmuir* **2008**, *24*, 8272–8279.
(40) Lee, H. J.; Yang, S. R.; An, E. J.; Kim, J. D. *Macromolecules* **2006**, *39*, 4938–4940.
(41) Hsu, Y. H.; Chiang, W. H.; Chen, M. C.; Chern, C. S.; Chiu, H. C. *Langmuir* **2006**, *22*, 6764.
(42) Puskas, J. E.; Chen, Y. *Biomacromolecules* **2004**, *5*, 1141–1154.
(43) Puskas, J. E.; Chen, Y.; Dahman, Y.; Padavan, D. *J. Polym. Sci., Part A: Polym. Chem.* **2004**, *42*, 3091–3109.
(44) Pinchuk, L.; Wilson, G. J.; Barry, J. J.; Schoephoersterd, R. T.; Parele, J. M.; Kennedy, J. P. *Biomaterials* **2008**, *29*, 448–460.
(45) Acosta, A. C.; Espana, E. M.; Yamamoto, H.; Davis, S.; Pinchuk, L.; Weber, B. A.; Orozco, M.; Dubovy, S.; Fantes, F.; Parele, J. M. *Arch. Ophthalmol.* **2006**, *124*, 1742–1749.
(46) Gallocher, S. L.; Aguirre, A.; Kasyanov, V.; Pinchuk, L.; Schoephoersterd, R. T. *J. Biomed. Mater. Res. B. Appl. Biomater.* **2006**, *79*, 325–334.
(47) Isayeva, I. S.; Kasibhatla, B. T.; Rosenthal, K. S.; Kennedy, J. P. *Biomaterials* **2003**, *24*, 3483–3491.
(48) Cadieux, P.; Watterson, J. D.; Denstedt, J.; Harbottles, R. R.; Puskas, J. E.; Howard, J.; Gan, B. S.; Reid, G. *Colloids Surf., B* **2003**, *28*, 95–105.
(49) Harris, M. J. *Poly(ethylene glycol) Chemistry: Biotechnical and Biomedical Applications*; Plenum Press: New York, 1992.
(50) Andrade, J. D.; Hlady, V.; Jeon, S.; Glass, J. E., Ed.; American Chemical Society: Washington D.C., 1996; Vol. 248, pp 51−59.
(51) Leckband, D.; Sheth, S.; Halperin, A. *J. Biomater. Sci. Polym. Ed.* **1999**, *10*, 1125–1147.
(52) Hoffman, A. S. *J. Biomater. Sci. Polym. Ed.* **1999**, *10*, 1011–1014.

(53) Krishnan, S.; Weinman, C. J.; Ober, C. K. *J. Mater. Chem.* **2008**, *18*, 3405–3413.
(54) Kennedy, J. P.; Ivan, B. *Designed Polymers by Carbocationic Macromolecular Engineering: Theory and Practice*; Hanser: New-York, 1992.
(55) Kaszas, G.; Puskas, J. E.; Kennedy, J. P.; Chen, C. C. *J. Macromol. Sci., Chem.* **1989**, *A26*, 1099–1114.
(56) Gao, B.; Kops, J. *Polym. Bull.* **1995**, *34*, 279–286.
(57) Rooney, J. M. *J. Polym. Sci., Part A: Polym. Chem.* **1981**, *19*, 2119–2122.
(58) Kurian, P.; Zschoche, S.; Kennedy, J. P. *J. Polym. Sci., Part A: Polym. Chem.* **2000**, *38*, 3200–3209.
(59) Yamashita, S.; Kodama, K.; Ikeda, Y.; Kohjiya, S. *J. Polym. Sci. Part. A Polym. Chem.* **1993**, *31*, 2437–2444.
(60) McLean, J. K.; Guillen-Castellanos, S. A.; Parent, J. S.; Whitney, R. A.; Resendes, R. *Eur. Polym. J.* **2007**, *43*, 4619–4627.
(61) McLean, J. K.; Guillen-Castellanos, S. A.; Parent, J. S.; Whitney, R. A.; Kulbaba, K.; Osman, A. *Ind. Eng. Chem. Res.* **2009**, *48*, 10759–10764.
(62) Parent, J. S.; Malmberg, S.; McLean, J. K.; Whitney, R. A. *Eur. Polym. J.* **2010**, *46*, 702–708.
(63) Bonduelle, C.; Gillies, E. R. *Macromolecules* **2010**, *43*, 9230–9233.
(64) Guillen-Castellanos, S. A.; Parent, J. S.; Whitney, R. A. *Macromolecules* **2006**, *39*, 2514–2520.
(65) Guillen-Castellanos, S. A.; Parent, J. S.; Whitney, R. A. *J. Polym. Sci. Part. A: Polym. Chem.* **2006**, *44*, 983–992.
(66) Ikeda, Y.; Kodama, K.; Kajiwara, K.; Kohjiya, S. *J. Polym. Sci. Part. B: Polym. Phys.* **1995**, *33*, 387–394.
(67) Strawhecker, K. E.; Kumar, S. K.; Douglas, J. F.; Karim, A. *Macromolecules* **2001**, *34*, 4669–4672.
(68) Model, M. A.; Healy, K. E. *J. Biomed. Mater. Res.* **2000**, *50*, 90–96.
(69) Lau, K. H. A.; Bang, J.; Hawker, C. J.; Kim, D. H.; Knoll, W. *Biomacromolecules* **2009**, *10*, 1061–1066.
(70) Zemła, J.; Lekka, M.; Raczkowska, J.; Bernasik, A.; Rysz, J.; Budkowski, A. *Biomacromolecules* **2009**, *10*, 2101–2109.
(71) Bonduelle, C. V.; Lau, W. M.; Gillies, E. R. *ACS Appl. Mater. Interfaces* **2011**, *3*, 1740–1748.
(72) Heriot, S. Y.; Jones, R. A. L. *Nature Mat.* **2005**, *4*, 782–786.
(73) Scriven, L. E.; Sternling, C. V. *Nature* **1960**, *187*, 186–188.